

An analytical model for electronic noise in a cryogenic bolometer detector readout circuit

V. Vatsa,^{a,b} A. Reza,^{c,1} A. Mazumdar,^{a,b,2} M. S. Pose,^c S. Mallikarjunachary,^c
 V. Nanal,^{c,3} R. G. Pillay,^d S. Ramakrishnan^{e,4} and A. Shrivastava^{a,f}

^a*Homi Bhabha National Institute,
 Mumbai-400094, India*

^b*INO, Tata Institute of Fundamental Research,
 Mumbai-400005, India*

^c*DNAP, Tata Institute of Fundamental Research,
 Mumbai-400005, India*

^d*Department of Physics, Indian Institute of Technology,
 Ropar-140001, India*

^e*DCMP&MS, Tata Institute of Fundamental Research,
 Mumbai-400005, India*

^f*Nuclear Physics Division, Bhabha Atomic Research Centre,
 Mumbai 400085, India*

E-mail: nanal@tifr.res.in

ABSTRACT: This paper presents an analytical model to quantify the measured noise in a cryogenic bolometer readout circuit. The model includes the contributions from the bias resistors and sensor resistors, voltage and current noise of amplifier, and cable capacitance. The model parameters are empirically estimated using frequency domain analysis of the measured noise data of indigenously developed Neutron Transmutation Doped (NTD) Ge sensors. The model is shown to describe noise data for NTD Ge sensors over a wide range of resistances corresponding to temperatures in the range 20 - 70 mK. Relative contributions of different components are discussed and it is shown that the contribution to the overall noise from the differential amplifier at 300 K is the dominant source. It is observed that the amplifier flicker noise is significantly lower than that specified in the amplifier datasheet. The present study also indicates that a desirable value of resistance of NTD sensor (R_{NTD}) from noise considerations is $\lesssim 1 \text{ G}\Omega$ at $\sim 20 \text{ mK}$.

KEYWORDS: Cryogenic detectors, Double-beta decay detectors, Front-end electronics for detector readout

¹Present address: Fermi National Accelerator Laboratory, Illinois-60510, USA

²Present address: Los Alamos National Laboratory, New Mexico-87545, USA

³Corresponding author

⁴Present address: Dept. of Physics, IISER Pune, Pune-411008, India

Contents

| | | |
|----------|---|-----------|
| 1 | Introduction | 1 |
| 2 | Analytical model for the bolometer noise | 3 |
| 3 | Noise measurements with NTD Ge sensors and SMD resistors | 5 |
| 3.1 | R_S and C_L measurement | 7 |
| 3.2 | Noise measurement | 8 |
| 4 | Optimization of model | 9 |
| 5 | Conclusion | 16 |

1 Introduction

A cryogenic bolometer detector offers an excellent energy resolution and high sensitivity, which makes it an ideal choice for several rare decay experiments such as neutrinoless double beta decay (NDBD) and dark matter searches [1]. Ideally the performance of a bolometer detector is expected to be superior due to its good intrinsic resolution.

However, in practice, resolution is often limited by the noise contributed from other sources [2]. Understanding these external noise contributions and mitigating the same is of paramount importance. Some of the major contributions arise from vibrations (e.g. pulse tube cooler [3, 4]), the Johnson noise in the sensor [5] and other electronic components in the bolometer readout circuit. Minimization of the electrical noise in the readout circuit has attracted much attention and the efforts have been concentrated towards the design of low noise preamplifier [6] and preamplifiers operating at low temperature [7]. The effect of external noise pickups on the performance of the bolometer is already reported in Ref. [8]. A typical readout circuit consists of a Neutron Transmutation Doped (NTD) Ge sensor at mK temperature, a current source for sensor biasing (generated by applying a constant voltage through a high bias resistor) and a front-end preamplifier. In order to understand the effect of noise from each of these sources and to predict the noise for a given readout circuit, a noise analysis of the bolometer readout circuit is required. An analytical noise model can also provide key information for the design and optimization of low noise readout circuitry for the bolometer.

A tin cryogenic bolometer detector (*TIN.TIN*-The INdia-based TIN detector) [9] is being developed to search for NDBD process in ^{124}Sn in the upcoming India-based Neutrino Observatory (INO). At Tata Institute of Fundamental Research, Mumbai, a prototype bolometer test setup with a sapphire absorber and indigenously fabricated NTD Ge sensor [10] has been developed for initial testing in a cryogen-free dilution refrigerator CFDR-1200 (Leiden Cryogenics) [11].

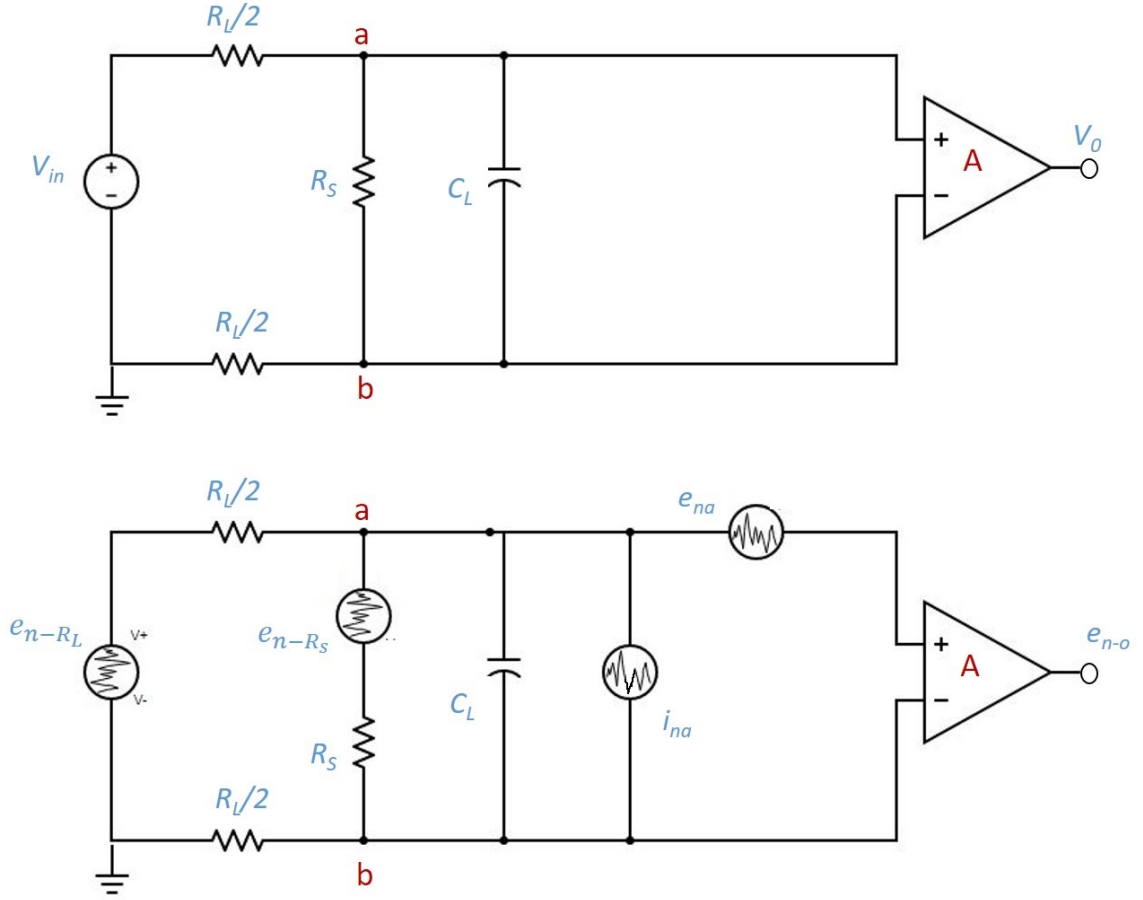


Figure 1. A bolometer readout circuit (top panel) and its equivalent noise model (bottom panel)

In this article, we present an analytical model for the estimation of electronic noise in a bolometer readout circuit. The model parameters are empirically determined from the fits to noise data of a family of NTD Ge sensors in a limited temperature range $T \sim 40 - 70$ mK. Since NTD Ge sensors have a limited operational range due to a very steep temperature dependence of R , noise measurements have also been carried out with standard surface mount device (SMD) resistors, where R values could be chosen flexibly to cover a higher temperature range. The simulated noise spectra with optimized parameters are compared with measured noise of NTD Ge sensors and SMD resistors. Further, it is shown that the amplifier noise is the predominant source in most cases. The analysis also shows that the R_{NTD} should be constrained below $1 \text{ G}\Omega$ to keep the thermal noise of the sensor as well as overall noise within acceptable limits.

2 Analytical model for the bolometer noise

The bolometer readout circuit and its equivalent noise model are shown in Figure 1. A pseudo-constant current source, consisting of a voltage source V_{in} in series with a high bias resistor R_L is used for sensor biasing. The voltage across the sensor is amplified using a low noise differential amplifier Femto DLPVA-100-F [12]. This amplifier, referred to as FEMTO hereafter, is characterised by low input voltage noise ($6.9 \text{ nV}/\sqrt{\text{Hz}}$), low input current noise ($1.6 \text{ fA}/\sqrt{\text{Hz}}$), variable gain (20-80 dB) and high input impedance ($1 \text{ T}\Omega$). It should be mentioned that although the current biasing scheme employs a unipolar power supply, the high CMRR (Common Mode Rejection Ratio) of 120 dB of FEMTO amplifier ensures that the common mode voltage is suppressed, and does not saturate its output. In principle, the unipolar supply can be replaced by a symmetric bipolar supply to improve the performance.

As is well known, the power density of noise is expressed as e_{rms}^2 per unit frequency (V^2/Hz). In the following, e_k represents the noise voltage contribution of the respective component, $\sqrt{(e_{k,rms}^2)B}$ in units of Volts, where B is the bandwidth in Hz. The Johnson thermal noise of the bias resistor R_L and the sensor resistor R_S are defined as:

$$e_{n-R_L} = \sqrt{4kT_L B R_L} \quad (2.1)$$

$$e_{n-R_S} = \sqrt{4kT_S B R_S} \quad (2.2)$$

where, T_L and T_S are temperatures (in Kelvin) of the bias and the sensor resistors, respectively, and k is Boltzman constant. It may be noted that the noise of the sensor bias voltage V_{in} i.e. of NI-DAQ card (PXI-6281) [13], specified to be $\sim 60 \text{ nV}/\sqrt{\text{Hz}}$ is negligible as compared to the thermal noise of bias resistor $\sim 57.5 \text{ }\mu\text{V}/\sqrt{\text{Hz}}$ for $R_L = 20 \text{ G}\Omega$ at room temperature and hence is not taken into consideration in the present work. Further, during the measurement and analysis, the acquisition bandwidth of FEMTO was kept at 1 kHz. The resolution bandwidth (B) is taken to be 0.1 Hz for consistency with the measured data, as explained in the later section. The contribution of noise at the input of the amplifier can be divided into four parts and each part can be calculated separately.

(a) Noise contribution (e_L) due to the bias resistor R_L :

$$\begin{aligned} e_L &= e_{n-R_L} \frac{R_S \parallel (1/j\omega C_L)}{R_L + [R_S \parallel (1/j\omega C_L)]} \\ &= \sqrt{4kT_L B R_L} \frac{R_S}{R_S + R_L + j\omega R_S R_L C_L} \end{aligned} \quad (2.3)$$

$$\begin{aligned} |e_L| &= \sqrt{4kT_L B R_L} \frac{R_S}{\sqrt{(R_S + R_L)^2 + (\omega R_S R_L C_L)^2}} \\ &= \sqrt{4kT_L B R_L} \frac{1}{R_L} \frac{R_{eq}}{\sqrt{1 + (\omega R_{eq} C_L)^2}} \end{aligned} \quad (2.4)$$

where R_{eq} is $R_S \parallel R_L$. The Eq. 2.4 depicts the behaviour of a low pass filter (LPF) with cutoff frequency $f_L = 1/2\pi R_{eq} C_L$. It can be seen from Eq. 2.4 that at $\omega = 0$, only a

small fraction ($R_S/(R_S+R_L)$) of thermal noise from R_L reaches the input of the amplifier. However, for $R_L = 20 \text{ G}\Omega$ at 300 K ($e_{n-R_L} = 18.2 \text{ }\mu\text{V}$) and $R_S = 500 \text{ M}\Omega$ (typical R_{NTD} at $T_S \sim 35 \text{ mK}$), the contribution of thermal noise from R_L at the input of the amplifier can be significantly larger ($\sim 0.44 \text{ }\mu\text{V}$). For a finite cable capacitance C_L , the noise contribution e_L reduces with increasing frequency.

(b) Noise contribution (e_S) due to the sensor resistance R_S :

$$\begin{aligned} e_S &= e_{n-R_S} \frac{R_L \|(1/j\omega C_L)}{R_S + [R_L \|(1/j\omega C_L)]} \\ &= \sqrt{4kT_S B R_S} \frac{R_L}{R_S + R_L + j\omega R_S R_L C_L} \end{aligned} \quad (2.5)$$

$$\begin{aligned} |e_S| &= \sqrt{4kT_S B R_S} \frac{R_L}{\sqrt{(R_S + R_L)^2 + (\omega R_S R_L C_L)^2}} \\ &= \sqrt{4kT_S B R_S} \frac{1}{R_S} \frac{R_{\text{eq}}}{\sqrt{1 + (\omega R_{\text{eq}} C_L)^2}} \end{aligned} \quad (2.6)$$

The Eq. 2.6 also depicts the behaviour of a LPF. Almost the entire fraction of thermal noise from R_S , ($R_L/(R_S+R_L) \sim 1$) appears at the input of the amplifier. In this case also, the e_S reduces with increasing frequency for a finite cable capacitance C_L .

(c) Noise contribution (e_{ni}) due to amplifier input current noise density i_{na} :

$$\begin{aligned} e_{ni} &= i_{na} \sqrt{B} [R_{\text{eq}} \|(1/j\omega C_L)] \\ &= i_{na} \sqrt{B} \frac{R_{\text{eq}}}{1 + j\omega R_{\text{eq}} C_L} \end{aligned} \quad (2.7)$$

$$|e_{ni}| = i_{na} \sqrt{B} \frac{R_{\text{eq}}}{\sqrt{1 + (\omega R_{\text{eq}} C_L)^2}} \quad (2.8)$$

Similar to e_S and e_L , the e_{ni} also has LPF like behaviour. In the temperature range of interest, i.e. $T_S \lesssim 1 \text{ K}$, e_{ni} will be larger than e_S and e_L over the entire frequency range.

(d) Noise contribution (e_{na}) due to input voltage noise density:

The input voltage noise of the amplifier (e_{na}) has two parts, namely, white noise (a frequency independent noise) and the flicker noise (inversely proportional to frequency). The input voltage noise (e_{na}) can then be written as,

$$e_{na} = \sqrt{(e_{\text{white}}^2 + e_{\text{flicker}}^2) B} = e_{\text{white}} \sqrt{\left[1 + \left(\frac{f_c}{f}\right)^n\right] B} \quad (2.9)$$

where, e_{white} is a characteristic parameter of the amplifier, f_c is the flicker corner frequency and index n is in the range 1 to 2 for semiconductor based amplifiers [14]. It is evident from Eq. 2.9 that there is a strong frequency dependence for $f < f_c$ due the flicker noise component, while at higher frequencies ($f > f_c$) e_{na} approaches e_{white} . Although a \sqrt{T}

dependence for $1/f$ noise is reported in the literature [15], in the present study temperature independent value is assumed since the amplifier is kept at a fixed temperature ($T = 300$ K).

Considering all four components as described above, total noise at the input (e_{n-in}) and output (e_{n-o}) of the amplifier with voltage gain A can be written as,

$$e_{n-in} = \sqrt{e_L^2 + e_S^2 + e_{ni}^2 + e_{na}^2} \quad (2.10)$$

$$e_{n-o} = A\sqrt{e_L^2 + e_S^2 + e_{ni}^2 + e_{na}^2} \quad (2.11)$$

It should be mentioned that the sensor itself can contribute to the flicker noise, which is not considered here. Figure 2 shows calculated individual noise components as a function of frequency for $R_S = 25$ and 350 M Ω at $T_S = 50$ mK, employing parameters as per the FEMTO datasheet, namely, $e_{white} = 6.9$ nV/ $\sqrt{\text{Hz}}$, $f_c = 80$ Hz and $i_{na} = 1.6$ fA/ $\sqrt{\text{Hz}}$. The index of the flicker noise n is set to be 1 and $C_L = 1$ nF. It is evident from the figure that since $T_S < 1$ K, and $R_S \ll R_L$, e_S is smaller than e_L . Further, it can be seen that the e_S , e_L and e_{ni} fall off at higher frequency with the same slope, namely, f_L , the characteristic frequency of the LPF. However, the total input noise (e_{n-in}) curve can have multiple slopes resulting from the competition of the input current noise (f_L/f) and the flicker noise (f_c/f) terms. In Figure 2, the initial $1/f$ fall off at very low frequency ($f < 2$ Hz) results from the flicker noise f_c/f , which dominates the contribution of e_{na} at low frequencies. While for larger sensor resistance, namely, for $R_S \geq 100$ M Ω , the e_{ni} term dominates over e_{na} in the low frequency region yielding a flat top as seen in Figure 2b. At higher frequency, $f \gtrsim 500$ Hz, e_{white} is the only surviving component of the noise. Since amplifier characteristic parameters (i.e. e_{white} , f_c and i_{na}) are independent of frequency, variation of total input noise e_{n-in} and sensitivity to probe the individual noise components depend on R_S and T_S . For small R_S , the e_{ni} contributions is lower than e_{na} at all frequencies (see Figure 2a), while for high R_S the e_{ni} component exceeds the e_{na} at low frequencies. However, the value of R_S influences the f_L and therefore the total noise spectrum shows a dominant plateau at $f \leq f_L$, characteristic of e_{ni} (e.g. see Figure 2b) It should be pointed out that if f_c is similar to f_L , then it will be difficult to disentangle the flicker noise from the e_{ni} component.

3 Noise measurements with NTD Ge sensors and SMD resistors

Noise Measurements for NTD Ge sensors and SMD resistors were carried out in separate runs using the CFDR-1200 setup at TIFR. Four indigenously fabricated NTD Ge sensors (M713, M715, M716 and M720) were directly coupled to the copper holder using GE varnish (see Figure 3) and the setup was mounted on the mixing chamber stage of the CFDR-1200. All four sensors have similar carrier concentrations and are identical in dimension (1mm \times 1mm \times 1mm) and with face-type contact [16, 17]. A set of SMD resistors, selected from same manufacturing batch with similar packaging, and having resistance in the range $\sim 1 - 100$ M Ω at 300 K, with negative temperature coefficient (i.e. non-metallic behaviour) was chosen for noise measurements as a close match to NTD Ge for resistance variation with temperature. The SMD resistors were also mounted on a similar copper holder. The

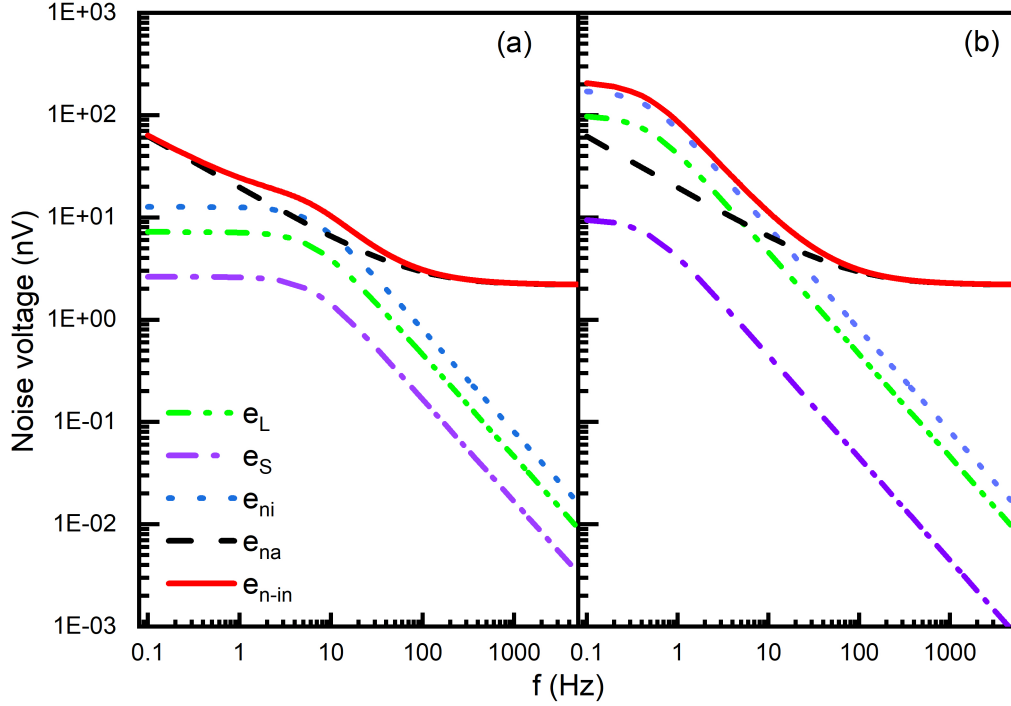


Figure 2. Different noise contributions at the amplifier input for a) $R_S = 25 \text{ M}\Omega$ at 50 mK and b) $R_S = 350 \text{ M}\Omega$ at 50 mK (see text for details)

mixing chamber was stabilized at the desired temperature during all the measurements. For simulating the noise in the readout circuit using the model described in the previous section, knowledge of R_S and C_L is an essential input. Measurements of R_S , C_L and noise are described in the following.

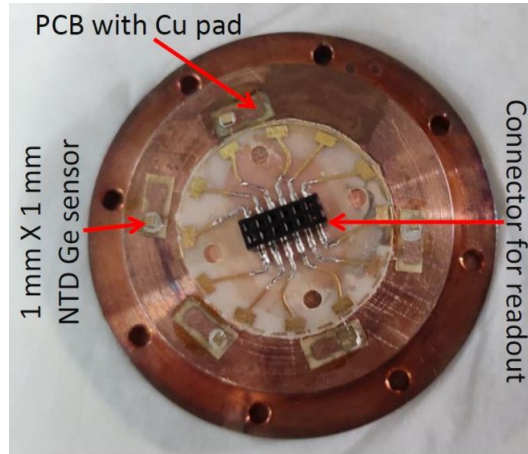


Figure 3. A picture of NTD Ge sensors mounted on copper holder for noise measurement at $T = 20 - 70 \text{ mK}$

3.1 R_S and C_L measurement

Sensor resistance measurements were done either with AVS-47B [18] resistance bridge (for $R_S < 2 \text{ M}\Omega$, typically $T_S > 100 \text{ mK}$) or with National Instrument-based Data Acquisition (NI PXI-6281 DAQ) system with FEMTO amplifier (for $R_S > 2 \text{ M}\Omega$, typically $T_S < 100 \text{ mK}$). In case of measurements with NI-DAQ, the sensor R_S was connected between the terminals 'a' and 'b' as shown in Figure 1 and a square wave excitation was applied to the sensor through a high bias resistor ($R_L=20 \text{ G}\Omega$) connected in series with the sensor. The amplitude of the input voltage was optimally chosen to get an acceptable signal to noise ratio (SNR), while minimizing the self heating of the sensor. The voltage response at output of the amplifier with gain $A = 60 \text{ dB}$, was recorded for a chain of 60 input voltage pulses. From the histogram of the output peak-to-peak voltage V_o recorded for all pulses, mean amplitude $\langle V_o \rangle$ was extracted and the sensor resistance was then calculated as

$$R_S = \frac{V_S}{V_{in} - V_S} \times R_L \quad (3.1)$$

where V_{in} is the voltage drop across $R_S + R_L$ and $V_S = \langle V_o \rangle / A$ is the voltage drop across the R_S .

For measurements with AVS-47B, the excitation voltage was fixed at a $30 \mu\text{V}$ and the data was averaged over 25 minutes. It can be seen from Figure 4 that resistances of all four NTD Ge sensors follow the expected Mott-like behaviour $R = R_0 \exp\left(\sqrt{\frac{T_0}{T}}\right)$ [19] with $\langle T_0 \rangle = 10.13 \pm 0.02 \text{ K}$ over a temperature range of 20 - 400 mK.

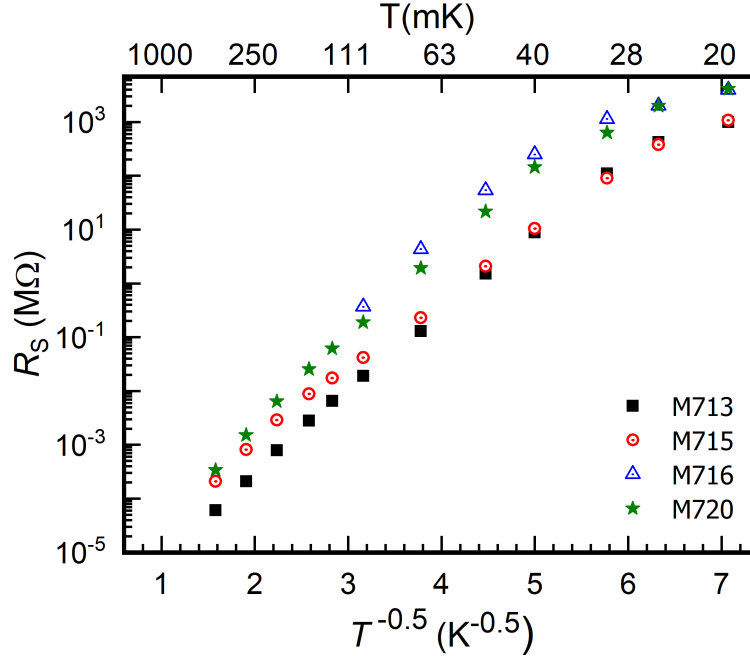


Figure 4. Variation of R_{NTD} as a function of T showing Mott behaviour.

The C_L was estimated by fitting the decay time (τ , i.e. RC time constant) of the falling edge of individual output pulses at the output of the amplifier (corresponding to the square wave input). As mentioned earlier, the measurements were done using very low bias voltage to avoid any self heating and hence the resistance was assumed to be a constant during the rise and fall of the square pulse excitation. A typical example of an exponential decay fit is shown in Figure 5. For each R_S at given T_S , average τ was obtained by fitting 12 pulses and the standard deviation (σ) is taken as the uncertainty. The mean capacitance $C_L = \tau_{mean}/R_S$, thus obtained are shown in Figure 6 for various R_S . For further analysis, C_L is taken to be 0.85 nF, which is the weighted mean for the NTD Ge sensor data. It was verified that simulated noise is not very sensitive to C_L and upto 20% variation in C_L did not produce any observable change in e_{n-o} .

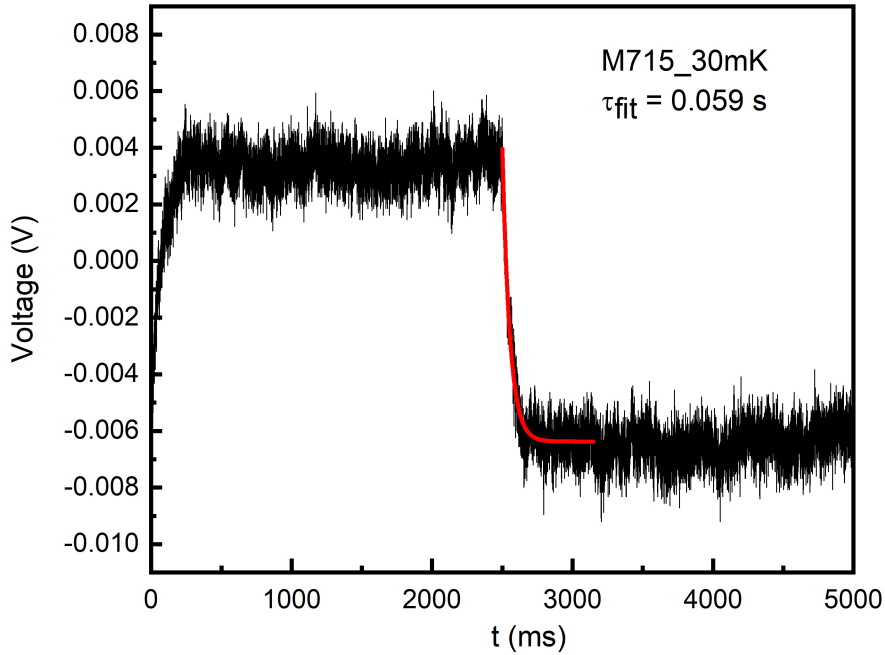


Figure 5. A typical example of an output waveform across the sensor resistor $R_S = 87 \text{ M}\Omega$. Exponential decay fit to the falling edge giving $\tau_{fit} = 0.059 \text{ s}$ corresponding to $C_L = 0.7 \text{ nF}$ is also shown.

3.2 Noise measurement

Noise measurements were done with NI DAQ over a temperature range of 20 - 70 mK for NTD Ge sensors, spanning a range of R_S over three orders of magnitude. A set of SMD resistors was selected to cover a similar range in R_S over a higher temperature range of $\sim 3 - 13 \text{ K}$. Ideally, noise measurements are done with zero bias voltage. However, a small DC voltage was applied to compensate any residual offset at output of the sensor arising due to thermoEMF [20] and other effects. A total of 100 k samples were acquired in a time window of 10 s using a sampling rate of 10 kHz, with bandwidth of the amplifier kept at 1 kHz. A typical 5 sec noise data for NTD Ge sensor M713 at $T = 20 \text{ mK}$ and at $T = 70 \text{ mK}$

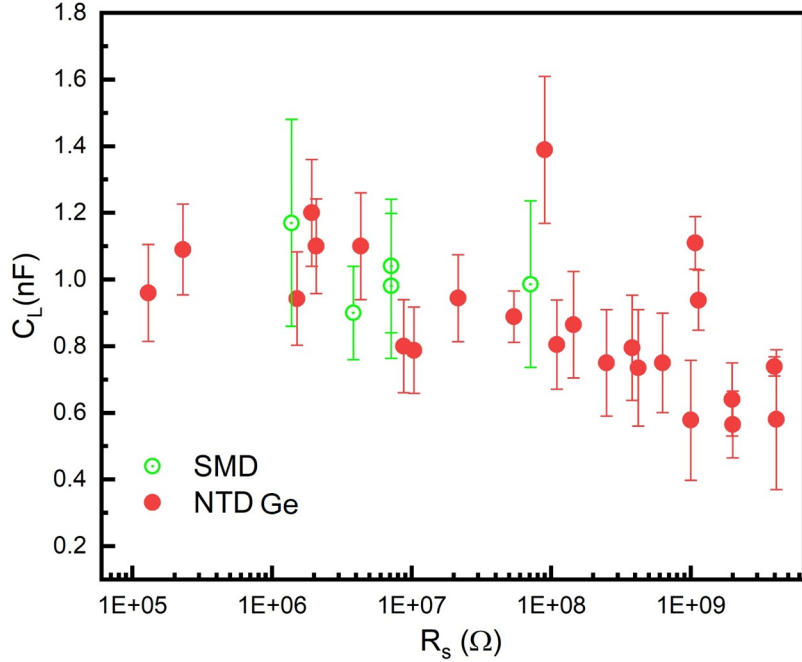


Figure 6. Distribution of estimated capacitance values for various R_S (SMD and NTD Ge sensors).

are shown in Figure 7. For each measurement (i.e. for given R_S , T_S), data were acquired in 12 time windows of 10 sec each (total length 120 s). The data in 12 time windows were averaged over to construct a single 10 s time domain data. It should be mentioned that at lower temperatures, drifts and wobbles in the baseline become visible, which correspond to ultra low frequency components and can be a limiting factor. Averaging over multiple time windows helps to improve the statistics.

4 Optimization of model

For further analysis and comparison with simulated noise spectra, 12 independently acquired 10 s long noise data were averaged to a single time window, to improve the statistics and thus the quality of the acquired data (as explained in the previous section). A discrete Fast Fourier Transform (FFT) of noise data was generated for the averaged 10 sec time data (as mentioned above) using a standard FFT algorithm and further analysis was carried out in frequency domain. The resolution bandwidth (B) for the FFT was set at 0.1 Hz and correspondingly time window was chosen to be 10 s. The simulated noise data was folded with a low pass filter function to take into the account the bandwidth of the amplifier (1 kHz). For a given R_S and T_S , the noise essentially depends on three parameters — i_{na} , f_c and e_{white} . Initial noise simulations were done with datasheet values for these parameters and two examples for different T_S and $R_S \sim$ few $M\Omega$ are shown in Figure 8. From the figure, it is evident that in low frequency window ($f < 10$ Hz), the model over-predicts the experimental data. Additionally, for $f_c = 80$ Hz (as per the datasheet) and $n = 1$, the

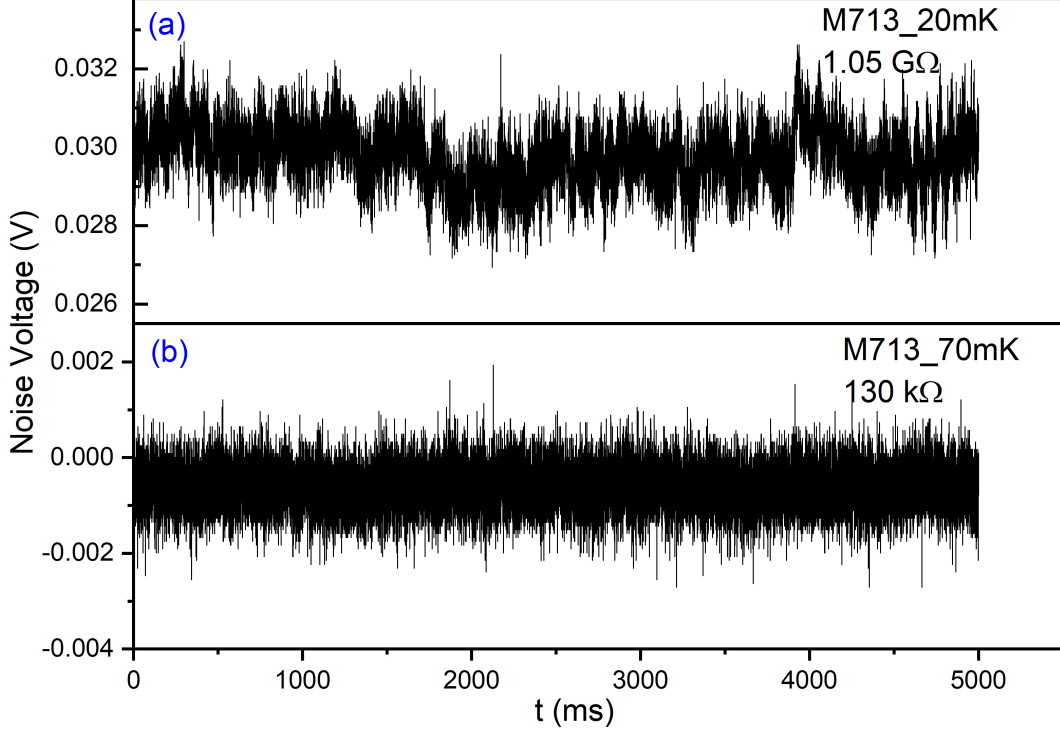


Figure 7. Typical noise data for NTD Ge sensor M713 at $T = 20$ mK (top panel) and $T = 70$ mK (bottom panel)

e_{na} will be the dominant contribution in the entire frequency region for $R_S \leq 100$ M Ω , and is expected to show $1/f$ behaviour till f_c . This behaviour is not observed in noise data at 40 - 50 mK, which shows a rather flat trend at low frequency (e.g. see Figure 8). In most of the data at $T \sim 50 - 70$ mK, where $R_S \leq 10$ M Ω , the initial $1/f$ component exhibits much smaller slope as compared to that expected for $f_c = 80$ Hz. Hence, an optimization of model parameters is needed for a better description of the data over a range of $R_S - T_S$. It should be mentioned that a few discrete peaks are also observed in the measured spectra at harmonics of 50 Hz, high frequency due to vacuum pumps & instrumentation, and in some cases harmonics of 1.4 Hz (frequency of the pulse tube cooler). However, these sharp noise peaks occurring at very specific frequencies do not influence the overall analysis of the underlying noise.

As seen from Figure 2, the parameter e_{white} corresponds to the saturation noise value at higher frequencies and can be unambiguously extracted irrespective of R_S and T_S . For extracting other two parameters (i.e. f_c and i_{na}), the R_S were carefully chosen to achieve maximum sensitivity for reliable fit, as explained earlier in the section 2. A total of 8 datasets of NTD Ge sensors with $R_S \sim 1 - 50$ M Ω and $T_S \sim 40 - 70$ mK were considered. The simulated noise was fitted to the experimental data in the frequency window 0.2 to 5000 Hz, after incorporating the amplifier response. The data at points $f = 0$ and 0.1 Hz were intentionally not included in the fitting region, since the first two points in the FFT can

be influenced by any residual DC offset in the time spectra. The fitting to simultaneously extract i_{na} , f_c and e_{white} was done using Root analysis framework [21].

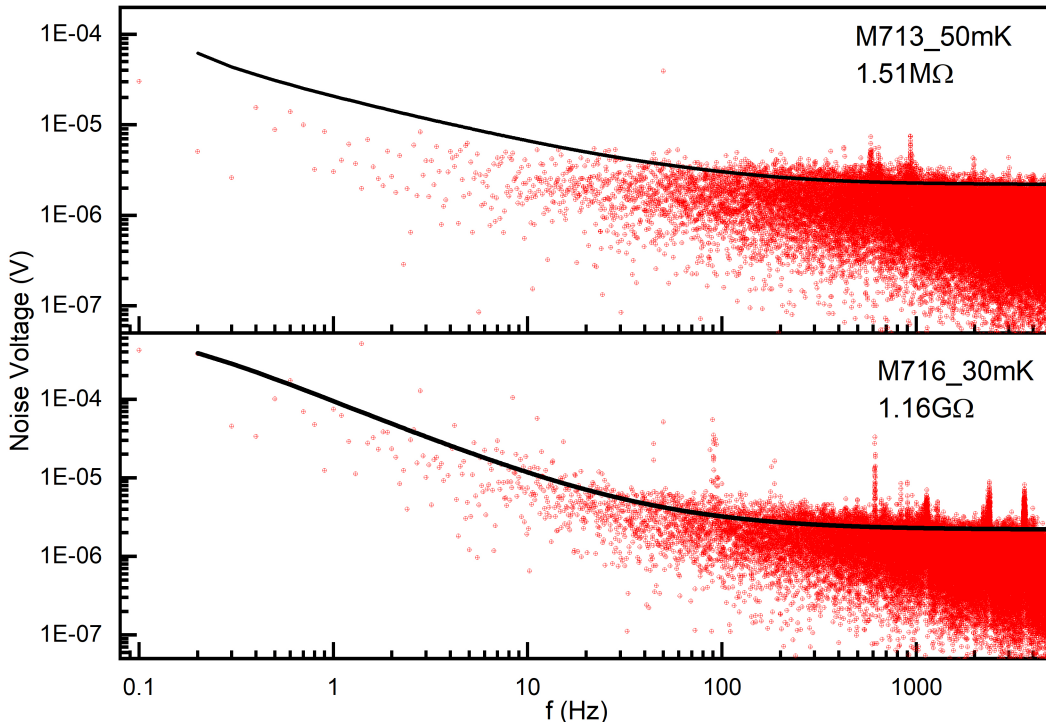


Figure 8. A comparison of simulated noise with parameters taken from the datasheet (solid black line) with measured noise data (red dots) for NTD Ge sensors. It is evident that $f_c = 80$ Hz over-predicts the noise at $f \lesssim 100$ Hz.

Figure 9 shows some of the data together with the best fit simulations. As mentioned earlier, the multiple slopes visible in simulated noise spectra result from competing amplitudes and slopes of f_c/f and f_L/f terms. For the datasets with $R_S \sim 1$ -10 M Ω at $T_S \sim 50$ - 70 mK, contributions of e_S and e_L are relatively small as compared to the other terms. The e_{na} term dominates over other contributions in the lower frequency window ($f < 2$ Hz) and hence is strongly sensitive to f_c . As e_{na} term decreases rapidly with increasing f , e_{ni} becomes a dominant contributor and leads to a flat noise in the 2-20 Hz window. The observed fall beyond this frequency is due to the f_L/f term. At $f > 1$ kHz, the amplifier bandwidth response results in the observed decreasing trend in the spectrum. It may be pointed out that in Figure 9(b, e), the f_L/f slope is not visible because of very small R_S .

Table 1 lists the extracted fit parameters with fitting errors and χ_{red}^2 . The χ_{red}^2 is computed as,

$$\chi_{red.}^2 = \frac{1}{N_{DF}} \sum_i \frac{1}{\sigma_i^2} [(e_{sim})_i - (e_{data})_i]^2 \quad (4.1)$$

where N_{DF} is number of degrees of freedom ($= 49997$), e_{sim} and e_{data} refer to simulated and measured noise voltage, respectively, in the i^{th} frequency bin. The σ_i is taken as e_{white}

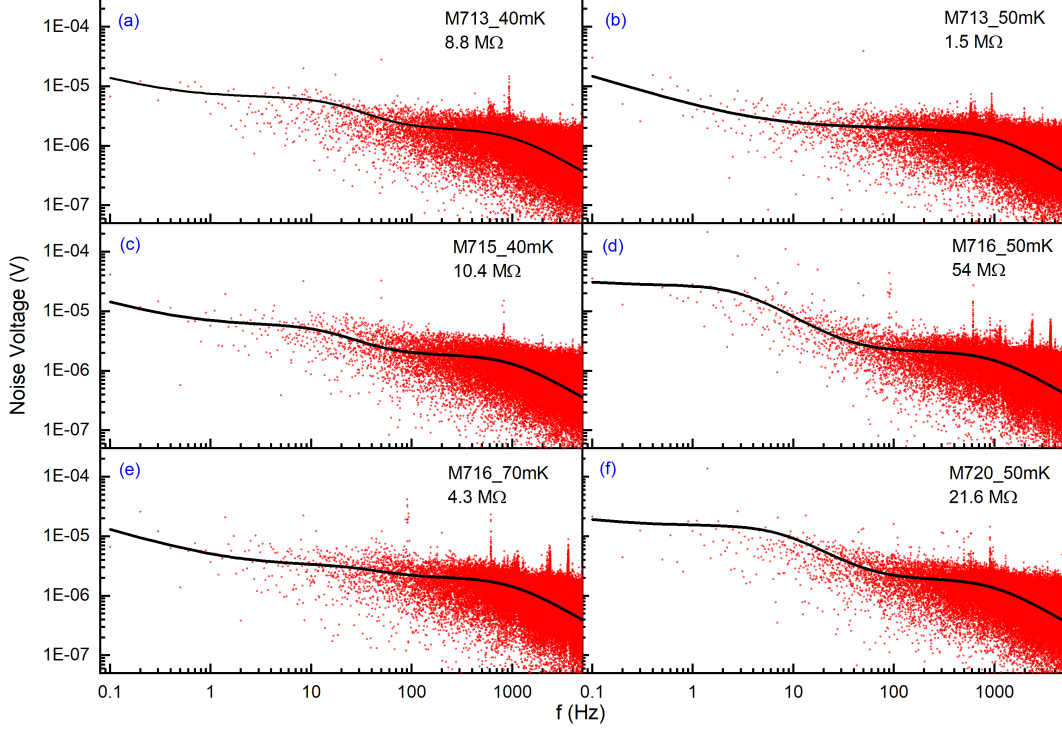


Figure 9. Simulated best fit noise curves (solid black line) with experimental data (red dots) for different NTD Ge sensors. Fit parameters are listed in Table 1 (see text for details).

Table 1. Model parameters obtained from fitting the NTD Ge sensor data

| Sensor Tag | R_S M Ω | f_c Hz | e_{white} nV/ \sqrt{Hz} | i_{na} fA/ \sqrt{Hz} | $\chi^2_{red.}$ |
|------------|---------------------|----------------|--------------------------------|-----------------------------|-----------------|
| M713_40mK | 8.8 | 4.2 ± 0.44 | 5.99 ± 0.021 | 1.95 ± 0.018 | 0.12 |
| M713_50mK | 1.5 | 3.9 ± 0.19 | 5.65 ± 0.018 | 2.15 ± 0.075 | 0.12 |
| M715_40mK | 10.4 | 5.3 ± 0.27 | 5.77 ± 0.018 | 1.28 ± 0.022 | 0.12 |
| M715_50mK | 2.1 | 4.4 ± 0.25 | 5.67 ± 0.020 | 1.04 ± 0.010 | 0.14 |
| M716_50mK | 54.0 | 4.5 ± 0.70 | 6.61 ± 0.230 | 1.30 ± 0.190 | 0.55 |
| M716_70mK | 4.3 | 3.9 ± 0.28 | 6.36 ± 0.023 | 1.25 ± 0.067 | 0.18 |
| M720_50mK | 21.6 | 3.9 ± 0.98 | 5.99 ± 0.032 | 1.97 ± 0.017 | 0.25 |
| M720_70mK | 1.9 | 4.5 ± 0.22 | 5.7 ± 0.018 | 2.15 ± 0.075 | 0.11 |
| Mean | | 4.3 ± 0.4 | 5.97 ± 0.05 | 1.63 ± 0.06 | |

(value obtained from the fit), which reflects the noise fluctuation in each bin.

The mean values for f_c , f_{white} and i_{na} listed at the bottom of the table are taken as optimal values for further simulations. It is important to note that e_{white} and i_{na} are similar to datasheet values, but the f_c value is drastically lower. The reason for this discrepancy is not understood. It should be mentioned that independent measurements of FEMTO

DLPVA-100F were also performed with low value resistors (1, 10 and 100 Ω) connected at the input, which also yielded $f_c \sim 4$ Hz.

To verify the model, the simulated noise spectra with these optimized parameters were compared with various NTD Ge sensor and SMD resistor datasets at different temperatures. A few examples of simulated noise together with data for $R_S \sim 10 - 1000$ M Ω are shown in Figure 10.

The good agreement between data and simulations at a higher T_S value (3 K) is clearly visible in Figure 10a. The flat noise at lower frequency and subsequent fall in the data for $R_S = 71.3$ and 250 M Ω (panel b and c of Figure 10) are well reproduced by the simulation. Similarly, for high R_S value (Figure 10(d), 1 G Ω) the observed fall in data is duly described by the dominant noise term e_{ni} of the model.

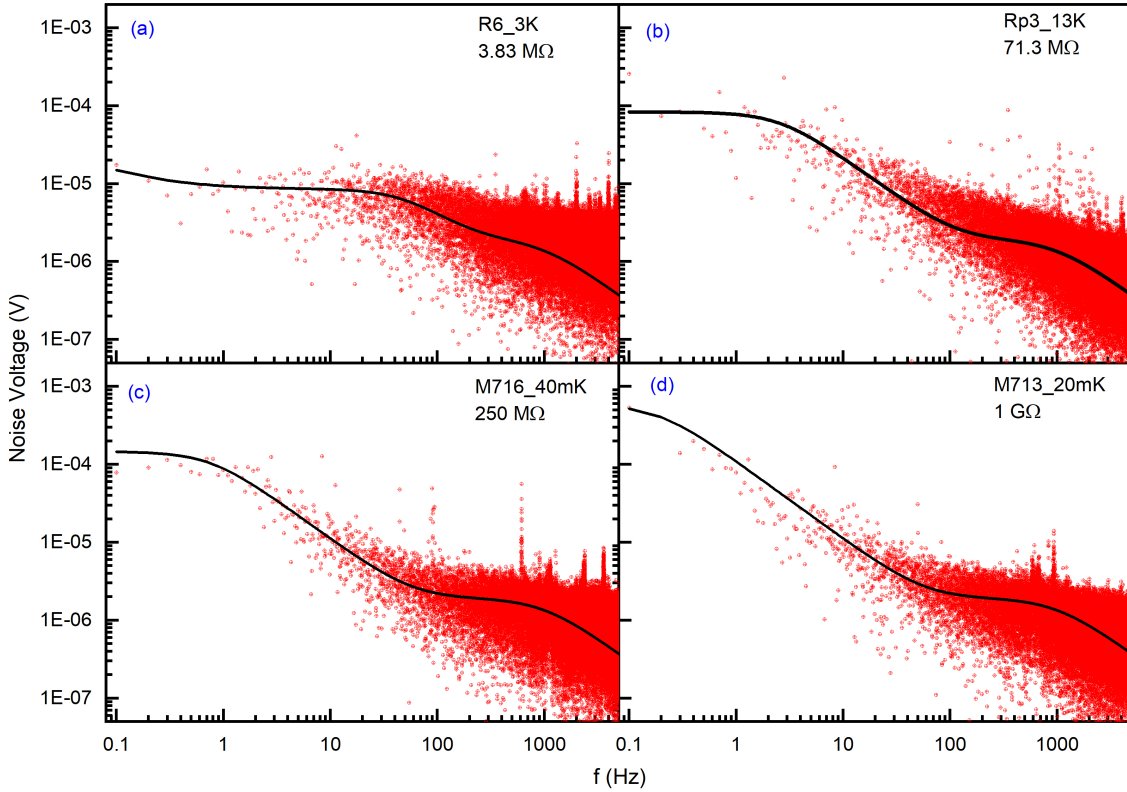


Figure 10. A comparison of simulated noise using optimized parameters ($f_c = 4.3$ Hz, $i_{na} = 1.63$ fA/ \sqrt{Hz} and $e_{white} = 5.97$ nV/ \sqrt{Hz}) and experimental data for various sensors in different $R_S - T_S$ range. Overall good agreement is visible (see text for details).

Another figure of merit for comparison of the data and simulation is the RMS value of noise voltage. From the model and data FFT spectrum, the RMS noise voltage e_{rms} is computed as

$$e_{rms} = \sqrt{\int_{f_l}^{f_h} \frac{e_i^2}{B} df} = \sqrt{\sum_i e_i^2} \quad (4.2)$$

where $(f_h - f_l)$ is the acquisition bandwidth of noise and df is the resolution bandwidth (which is same as B in the present case). Simulated and measured e_{rms} for frequency window 0.2 - 1000 Hz are given in the Table 2 for NTD Ge sensors spanning temperature range 20 to 70 mK. Additionally, to discount the effect of the DC offset and low frequency wobble in the experimental data, e_{rms} only in the 5.1 - 1000 Hz window is also shown. Table 3 shows data for SMD resistors in the temperature range 3 to 13 K. It should be mentioned that the flicker noise contribution in the SMD resistors is expected to be different from that in NTD Ge sensors, given the difference in the volume and packaging. However, for the range of $R - T$ under consideration, e_{ni} and e_S are the dominant terms and measured data is not sensitive to f_c . From both the tables it is evident that overall agreement between model and data (i.e. $< e_{rms}^{data} / e_{rms}^{sim} >$) is within 15% for the frequency range of 5.1-1000 Hz. Thus, it can be concluded that the analytical noise model with optimized parameters is able to describe data over a wide range of R_S and T_S .

Table 2. A comparison of simulated noise, e_{rms}^{sim} (with optimized parameters from Table 1) and measured data e_{rms}^{data} for NTD Ge sensors.

| sensor tag | R_S M Ω | e_{rms}^{sim} (mV) (0.2-1000)Hz | e_{rms}^{data} (mV) (0.2-1000)Hz | e_{rms}^{sim} (mV) (5.1-1000)Hz | e_{rms}^{data} (mV) (5.1-1000)Hz |
|------------|---------------------|--------------------------------------|---------------------------------------|--------------------------------------|---------------------------------------|
| M713_20mK | 1050 | 0.78 | 0.5 | 0.23 | 0.27 |
| M713_30mK | 111 | 0.37 | 0.35 | 0.23 | 0.23 |
| M713_70mK | 0.13 | 0.17 | 0.17 | 0.17 | 0.16 |
| M715_20mK | 1140 | 0.79 | 0.52 | 0.23 | 0.26 |
| M715_30mK | 90.4 | 0.34 | 0.34 | 0.23 | 0.28 |
| M715_70mK | 0.23 | 0.17 | 0.18 | 0.17 | 0.18 |
| M716_20mK | 4010 | 0.89 | 0.89 | 0.23 | 0.31 |
| M716_30mK | 1160 | 0.79 | 0.76 | 0.24 | 0.29 |
| M716_40mK | 250 | 0.5 | 0.67 | 0.23 | 0.31 |
| M720_20mK | 4100 | 0.88 | 2.07 | 0.24 | 0.28 |
| M720_30mK | 650 | 0.69 | 0.95 | 0.23 | 0.26 |
| M720_40mK | 145 | 0.41 | 0.69 | 0.22 | 0.24 |

As mentioned in section 2, the index n of the flicker frequency can take values between 1 to 2 and $n = 1$, which corresponds to the slowest fall, was used. It should be pointed out that index $n = 1$ and 2 effectively encompasses flicker and shot noise. To assess the impact of n on noise parameters, fitting was also done with $n=2$ in Eq. 2.9. It is observed that the parameters e_{white} and i_{na} are not influenced by choice of n , but f_c varies as expected. The simulated noise spectra with $n=1$ and 2 for best fit parameters are shown in Figure 11. It

Table 3. A comparison of simulated noise, e_{rms}^{sim} (with optimized parameters from Table 1) and measured data e_{rms}^{FFT} for SMD resistors.

| sensor tag | R_S M Ω | e_{rms}^{sim} (mV) (0.2-1000)Hz | e_{rms}^{data} (mV) (0.2-1000)Hz | e_{rms}^{sim} (mV) (5.1-1000)Hz | e_{rms}^{data} (mV) (5.1-1000)Hz |
|------------|---------------------|--------------------------------------|---------------------------------------|--------------------------------------|---------------------------------------|
| R6_3K | 3.83 | 0.28 | 0.36 | 0.27 | 0.36 |
| Rp1_13K | 1.38 | 0.46 | 0.44 | 0.46 | 0.44 |
| Rp2_13K | 7.15 | 0.49 | 0.54 | 0.47 | 0.52 |
| Rp3_13K | 71.3 | 0.55 | 0.60 | 0.34 | 0.43 |
| Rp6_13K | 7.15 | 0.49 | 0.49 | 0.46 | 0.47 |

can be seen that differences are visible only at very low frequency region ($f < 10$ Hz) and the e_{rms} values are nearly identical 0.173 and 0.177 mV for $n=1$ and 2, respectively. The present data cannot distinguish between $n=1$ or 2.

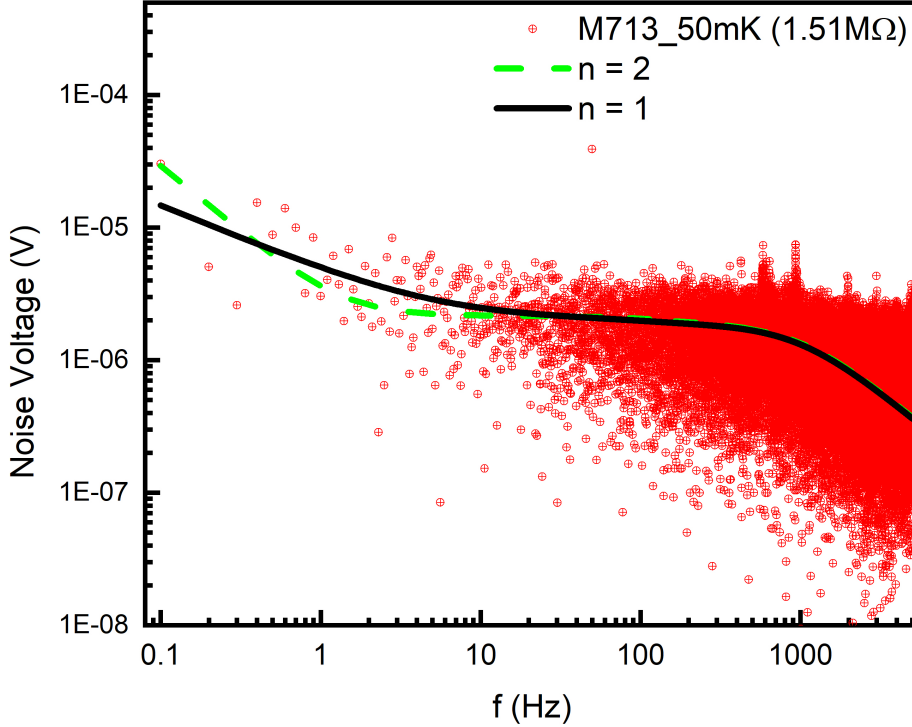


Figure 11. A comparison of simulated noise for flicker noise index $n = 1$ and 2 for $R_S = 1.51$ M Ω , $T_S = 50$ mK.

Except e_{na} other noise factors have R_S dependence, with e_{ni} as a leading term proportional to the R_S . A high value of R_S is essential for good sensitivity in the bolometer signal. However, readout circuit noise and noise due to other factors like harmonics of pulse tube cooler, vacuum pumps and instrumentation, etc. also increase with increasing sensor resistance. Thus, an optimal value of R_S is desirable to enhance the signal, while keeping

overall noise within acceptable window. Employing the present model, it is seen that for $R_S \lesssim 100 \text{ M}\Omega$, e_{na} is the dominant contribution at all frequencies. While for $R_S \gtrsim 100 \text{ M}\Omega$ both e_{ni} and e_L will be dominant factors. However, for $R_S \sim 100 - 350 \text{ M}\Omega$ the e_{ni} and e_{na} contributions will be of the similar magnitude at low frequency. For $R_{NTD} \sim 1 \text{ G}\Omega$, the expected noise is shown in Figure 12, which gives $e_{rms}^{sim} \sim 0.5 \text{ mV}$ at the amplifier output. Hence, from noise point of view it is suggested that R_{NTD} should be smaller than $1 \text{ G}\Omega$. Since the dependence of the resistance of NTD Ge sensor on temperature is described by Mott behaviour (see section 3.1), the sensitivity of NTD Ge sensor [22] i.e. $\frac{dR}{dT}$ is proportional to $R_S \sqrt{\frac{T_0}{T}}$. Therefore, for better sensitivity, large R_s is desirable. Thus, R_{NTD} in the range of $0.5 - 1 \text{ G}\Omega$ will be preferable to achieve a good sensitivity and low noise.

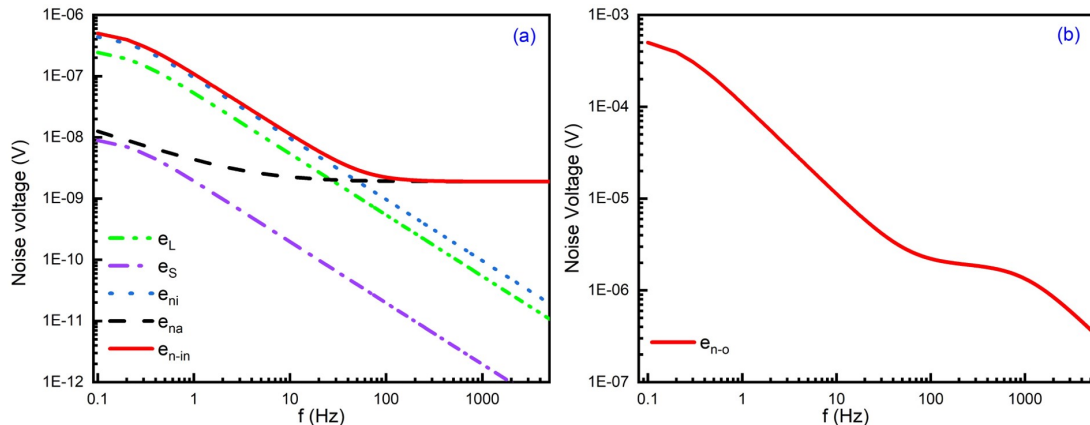


Figure 12. Simulated noise spectrum for $R_{NTD} = 1 \text{ G}\Omega$ at 20 mK with optimized parameters: (a) individual contributions and total noise at the amplifier input, (b) total noise at the amplifier output (inclusive of the amplifier response)

5 Conclusion

An analytical model for bolometer readout circuit has been presented to understand the effect of noise from different circuit components. The parameters of the model (e_{white} , i_{na} and f_c) have been optimized to fit the observed data of NTD Ge sensors. While empirical values of the parameters e_{white} , i_{na} are consistent with the datasheet values, the flicker corner frequency f_c is observed to be significantly smaller (4.3 Hz) than the specified value of 80 Hz . The optimized model has been tested for NTD Ge sensors over a wide range of $R_S = 130 \text{ k}\Omega - 4.1 \text{ G}\Omega$ in $20 - 70 \text{ mK}$ and for SMD resistors in the range $T = 3 - 13 \text{ K}$, and is found to describe FFT of the measured data very well. The model can be used to predict the value of voltage noise e_{rms} . The model is general enough and can be extended to any bolometer readout circuit or amplifier. From noise considerations, the desired range for resistance of NTD Ge sensor is shown to be $0.5 - 1 \text{ G}\Omega$. Further, it is shown that the current noise from amplifier is the leading source of the noise for the relevant range of $R_S \sim 350 - 1000 \text{ M}\Omega$ for NTD Ge sensor below 100 mK . Consequently, A suitable

low temperature amplifier ($\sim 100 - 120$ K) with small i_{na} and low f_c is desirable for the cryogenic bolometer readout.

Acknowledgments

We thank Mr. K. V. Divekar for assistance during measurements. This work is supported by the Department of Atomic Energy, Government of India, under Project No. RTI4002.

References

- [1] P. F. de Salas, S. Gariazzo, *et al.*, *Neutrino Mass Ordering from Oscillations and Beyond: 2018 Status and Future Prospects*, *Front. Astron. Space Sci.* **5**, (2018) 36.
- [2] C. Enss and D. McCammon, *Physical Principles of Low Temperature Detectors: Ultimate Performance Limits and Current Detector Capabilities*, *J. Low Temp. Phys.* **151**, (2008) 5–24.
- [3] A. M. J. den Haan, *et al.*, *Atomic resolution scanning tunneling microscopy in a cryogen free dilution refrigerator at 15 mK*, *Rev. Sci. Instrum.* **85**, (2014) 035112.
- [4] A. D’Addabbo, C. Bucci, L. Canonica *et al.*, *An active noise cancellation technique for the CUORE Pulse Tube cryocoolers*, *Cryogenics* **93**, (2018) 56–65.
- [5] M Carrettoni and M Vignati, *Signal and noise simulation of CUORE bolometric detectors*, *JINST*, **6**, (2011) P08007
- [6] Ilya L. Novikov, Boris I. Ivanov *et al.*, *Cryogenic low-noise amplifiers for measurements with superconducting detectors*, *J. of Nanotechnology* **11**, (2020) 1316-1320
- [7] A. Reza, V. Vatsa *et al.*, *A Cryogenic Front-End Preamplifier Operating at 120 K for Bolometric Detector*, *J Low Temp Phys* **199**, (2020) 200–205
- [8] A. Garai *et al.*, *Study of the effect of external noise pickups on the performance of a cryogenic bolometer*, *Rev. Sci. Instrum.* **90**, (2019) 096104.
- [9] V. Nanal, *Search for neutrinoless double beta decay in ^{124}Sn* , *EPJ Web Conf.* **66**, (2014) 08005.
- [10] A. Garai *et al.*, *A pulse height analysis technique for cryogenic bolometers*, *J. Low Temp. Phys.* **184**, (2016) 609–614.
- [11] V. Singh, S. Mathimalar *et al.*, *Cryogen-free dilution refrigerator for bolometric search of neutrinoless double beta decay ($0\nu\beta\beta$) in ^{124}Sn* , *Pramana* **81**, (2013) 719–725
- [12] <https://www.femto.de/images/pdf-dokumente/de-dlpva-100-f.pdf>
- [13] <https://www.ni.com/docs/en-US/bundle/pci-pxi-usb-6281-specs/page/specs.html>
- [14] A. Van Der Ziel, *Advances in Electronics and Electron Physics*, **49**, (1979) 225-297.
- [15] Richard F. Voss and John Clarke, *Flicker($1/f$) noise: Equilibrium temperature and resistance fluctuations*, *Phys. Rev. B* **B**, (1976) 556-573.
- [16] V. Vatsa *et al.*, *Influence of contact geometry on NTD sensor performance*, *IEEE 14th Workshop on Low Temperature Electronics (WOLTE)*, (2021) 1-4.
- [17] V. Vatsa *et al.*, “Performance of NTD Ge sensors with face-contacts”, TIN.TIN Collaboration Notes, (2020) 2020-003

https://www.tifr.res.in/~tin.tin/publications/TinTin2020_003_vatsa.pdf

- [18] http://www.picowatt.fi/support/avs47bmanual_20080411.pdf
- [19] A.L. Efros and B.I. Shklovskii, *Coulomb gap and low temperature conductivity of disordered systems*, *J. Phys. C: Solid State Physics* **8** (1975) L49
- [20] Kamran Behnia, *Fundamentals of Thermoelectricity*, *Oxford University Press*, (2015).
- [21] <https://root.cern/>
- [22] Wataru Ootani *et al.*, *Sensitive germanium thermistors for cryogenic thermal detector of Tokyo dark matter search programme*, *CERN Document server*, (1995) 290269.